AIAA JOURNAL
Vol. 33, No. 2, February 1995

Compressive Buckling of Rectangular Composite Plates with a Free-Edge Delamination

Hiroshi Suemasu,* Katsuhisa Gozu,† and Kunio Hayashi‡
Sophia University, Tokyo 102, Japan
and
Takashi Ishikawa§
National Aerospace Laboratory, Tokyo 181, Japan

An experimental and analytical investigation is conducted on the compressive buckling behavior of orthotropic plates with a delamination. The plates, which have three simply supported edges and one free edge, are a simplified model of stiffener plates of a stiffened panel. A uniform width delamination is located at their free edges over the whole length. In the analysis, the Rayleigh–Ritz approximation method is adopted. A constrained point is introduced to allow the contact between the two delaminated surfaces. Imaginary springs about relative displacement and two relative slopes are introduced at the constrained point. With the constraint, buckling loads of physically admissible buckling modes can be obtained by ordinary buckling analysis. The global buckling load reduction is found to be significant and almost proportional to the delamination width. Local delamination buckling is found to occur when the delamination is located near the surface and its size is relatively large compared with that of the plate. The local buckling mode is different from the global one, and more wave number in loading direction and constrained points are necessary to obtain physically admissible solutions. The analytical results agree well with the experimental ones.

I. Introduction

FIBER-REINFORCED composite laminates attract intensive attentions as promising candidates of a future material not only in aerospace engineering but also in various engineering fields owing to their remarkable properties such as high strength and high stiffness-to-weight ratios, good fatigue resistance, possibility of tailoring, etc. Interlaminar delamination, which is suspected to occur owing to impact load, fatigue, etc., is one of typical damage patterns of laminated structures. Its introduction causes significant reduction of compressive strength of the plates. Therefore, a lot of studies have been performed to disclose the effects of the delamination(s), particularly on one-dimensional models[1–10] and have shown the possibility of a serious reduction of compressive strength, that is, low buckling load and delamination propagation due to postbuckling deformation. Analytical studies on the effect of delaminations on the compressive behavior of two-dimensional plates are limited only to special cases.[11–15]

The delamination is also thought to appear at a free edge of stiffener plates of stiffened panels and to reduce significantly its compressive strength. The panel is modeled as a plate with three simply supported edges and one free edge. There may also occur a contact problem. When the contact area is small compared with the delaminated area, the effect of the contact area may be approximated a concentrated force. Based on this idea, the problem has been analyzed through an introduction of a constrained point,[10,13,14] where relative displacement and slopes of the delaminated surface are restricted. The contact problem has also been well treated by an introduction of a nonlinear distributed spring with a switching function on the plate surface proposed by Shahwan and Waas.[16] The constrained point is modified by using imaginary springs in relative displacement and slopes at the contact area to conform to the usual eigenvalue program. Compressive buckling loads and mode shapes of the orthotropic plate are obtained by an eigenvalue analysis and compared with experimental results.

II. Theory

A. Buckling Equation

A compressive buckling behavior of a rectangular plate with three simply supported edges and one free edge is examined. Figure 1 shows a coordinate system and the delaminated region. The properties of the plate are assumed to be homogeneous in the thickness direction, that is, no bending-stretching coupling is considered even in the delaminated area. A uniform width delamination is assumed to be located along the free edge. The boundary conditions are

$$u = \tau_{xy} = 0, \quad w = M_x = 0 \qquad \text{on } x = 0 \tag{1}$$

$$\sigma_x = \tau_{xy} = 0, \quad Q_z = M_x = 0 \qquad \text{on } x = a \tag{2}$$

$$v = \tau_{xy} = 0, \quad w = M_y = 0 \qquad \text{on } y = 0 \tag{3}$$

$$v = -\varepsilon_0 b, \quad \tau_{xy} = 0, \quad w = M_y = 0 \qquad \text{on } y = b \tag{4}$$

where u, v, and w denote, respectively, displacements in x, y, and z directions, and a and b are the width and length of the plate. The term τ_{xy} is a shear stress in the x-y plane. The notations Q_z, M_x, and M_y are a transverse shear force and bending moments in x and y directions. The value ε_0 is a normalized displacement of the loading edge.

When the transverse shear deformation is neglected and the plate is long, the compressive buckling stress σ_{cr} of the present plate without a delamination is approximately written as

$$\sigma_{cr} = \frac{1}{b^2 h}\left[(\pi\lambda)^2 D_{22} + 12 D_{66}\right] \tag{5}$$

where h is the plate thickness, $\lambda = b/a$ is the aspect ratio of the panel, and the coefficients D_{22}, and D_{66} are the components of the

Received March 22, 1994; presented in part at the AIAA 35th Structures, Structural Dynamics, and Materials Conference, Hilton Head, SC, April 18–20, 1994; revision received Sept. 25, 1994; accepted for publication Sept. 25, 1994.

*Associate Professor, Department of Mechanical Engineering, Faculty of Science and Technology, 7-1 Kioicho, Chiyodaku. Member AIAA.

†Research Associate, Department of Mechanical Engineering, Faculty of Science and Technology, 7-1 Kioicho, Chiyodaku.

‡Professor, Department of Mechanical Engineering, Faculty of Science and Technology, 7-1 Kioicho, Chiyodaku.

§Senior Research Officer, Mitaka-Shi. Member AIAA.

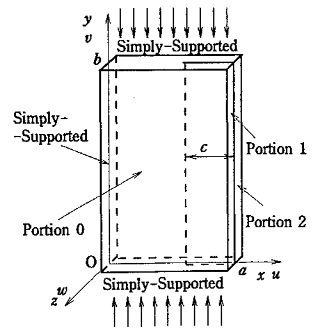

Fig. 1 Analytical model.

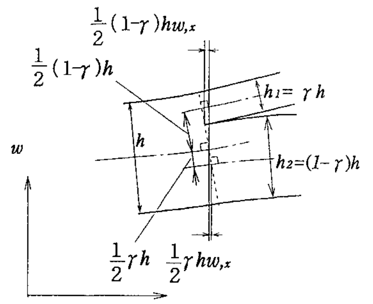

Fig. 2 Continuity condition of the displacements at the delamination front.

bending stiffness matrix of the laminate. The component D_{11}, the bending stiffness in transverse direction to the load, does not appear in the expression of the buckling stress of Eq. (5). The buckling mode has only one half wave regardless of the aspect ratio of the plate.

The Kirchhoff hypothesis is assumed to hold even in the neighborhood of the delamination front as shown in Fig. 2. The continuity condition of the displacements at the edge of the delamination $x = a - c$ can be written simply with the displacements of the midplanes of each delaminated and undelaminated portions:

$$\begin{aligned} w_I &= w_0 \\ w_I,_x &= w_0,_x \\ w_I,_y &= w_0,_y \end{aligned} \tag{6}$$

$$\begin{aligned} u_I + hk_I w_0,_x &= u_0 \\ v_I + hk_I w_0,_y &= v_0 \end{aligned} \tag{7}$$

where $I = 1$ and 2.

$$k_1 = -\tfrac{1}{2}(1-\gamma), \qquad k_2 = \tfrac{1}{2}\gamma$$

where $\gamma = h_1/h$ is a normalized thickness of the thinner delaminated portion. The subscripts 0, 1, and 2 following u, v, and w denote the undelaminated and two delaminated portions.

The Rayleigh-Ritz method is applied to obtain approximated values of the buckling loads and corresponding buckling modes. The displacements are developed with the global and local mode functions to satisfy the boundary and continuity conditions. The local functions have values only in the delaminated portion and zero in the undelaminated portion:

$$\frac{w_I}{h} = q_m\phi_m(\xi,\eta) + q_m{}^{(I)}\bar{\phi}_m(\xi,\eta) \tag{8}$$

$$\frac{a}{h^2}u_I = \nu_{xy}S\xi + k_I q_m f_m(\eta) + U_m\psi_m(\xi,\eta) + U_m{}^{(I)}\bar{\psi}_m(\xi,\eta) \tag{9}$$

$$\frac{b}{h^2}v_I = -S\eta + k_I q_m g_m(\eta) + V_m\varphi_m(\xi,\eta) + U_m{}^{(I)}\bar{\varphi}_m(\xi,\eta) \tag{10}$$

where $\xi = x/a$ and $\eta = y/b$. The parameter S is a nondimensional displacement of the loading edge:

$$S = \left(\frac{b}{h}\right)^2 \varepsilon_0 \tag{11}$$

The summation convention rule is used. The mode functions have the following forms:

$$\phi_m(\xi,\eta) = P_{2k_m-1}(\xi)\sin\pi l_m\eta$$

$$\bar{\phi}_m(\xi,\eta) = \begin{cases} \bar{\xi}P_{2k_m-1}(\bar{\xi})\vartheta_{l_m}(\eta) & \bar{\alpha} < \xi < 1 \\ 0 & 0 < \xi < \bar{\alpha} \end{cases}$$

$$\vartheta_j(\eta) = \cos\pi(j-1)\eta - \cos\pi(j+1)\eta$$

$$f_m(\eta) = \phi_m,_\xi(\bar{\alpha},\eta)$$

$$g_m(\eta) = \phi_m,_\eta(\bar{\alpha},\eta)$$

$$\psi_m(\xi,\eta) = P_{2k_m-1}(\xi)\cos\pi(l_m-1)\eta$$

$$\bar{\psi}_m(\xi,\eta) = \begin{cases} P_{2k_m-1}(\bar{\xi})\cos\pi(l_m-1)\eta & \bar{\alpha} < \xi < 1 \\ 0 & 0 < \xi < \bar{\alpha} \end{cases}$$

$$\varphi_m(\xi,\eta) = P_{2k_m-1}(\xi)\sin\pi l_m\eta$$

$$\bar{\varphi}_m(\xi,\eta) = \begin{cases} P_{2k_m-1}(\bar{\xi})\sin\pi l_m\eta & \bar{\alpha} < \xi < 1 \\ 0 & 0 < \xi < \bar{\alpha} \end{cases}$$

where $\bar{\alpha} = 1 - \alpha$ and $\alpha = c/a$ is a normalized delamination width. The function P_m is the mth Legendre polynomial. The suffices k_m and l_m mean the wave numbers in x and y directions of mth mode functions. Of course, the local mode functions $\bar{\phi}_m$, $\bar{\psi}_m$, and $\bar{\varphi}_m$ are not zero only in the region $\bar{\alpha} < \xi < 1$. The strains are expressed with the generalized coordinates:

$$\kappa_x^{(I)} = -w,_{xx}^{(I)} = -\frac{h}{a^2}\left[q_m\phi_m,_{\xi\xi} + q_m^{(I)}\bar{\phi}_m,_{\xi\xi}\right] \tag{12}$$

$$\kappa_y^{(I)} = -w,_{yy}^{(I)} = -\frac{h}{b^2}\left[q_m\phi_m,_{\eta\eta} + q_m^{(I)}\bar{\phi}_m,_{\eta\eta}\right] \tag{13}$$

$$\kappa_{xy}^{(I)} = -w,_{xy}^{(I)} = -\frac{h}{ab}\left[q_m\phi_m,_{\xi\eta} + q_m^{(I)}\bar{\phi}_m,_{\xi\eta}\right] \tag{14}$$

$$\begin{aligned} \varepsilon_x^{(I)} &= u,_x^{(I)} + \tfrac{1}{2}\left[w,_x^{(I)}\right]^2 \\ &= -\left(\frac{h}{a}\right)^2 \Big\{\nu\lambda^{-2}S + U_m\psi,_\xi + U_m^{(I)}\bar{\psi},_\xi \\ &\quad + \tfrac{1}{2}\big[q_m q_n\phi_m,_\xi\,\phi_n,_\xi + q_m q_n^{(I)}\phi_m,_\xi\,\bar{\phi}_n,_\xi \\ &\quad + q_m^{(I)}q_n\bar{\phi}_m,_\xi\,\phi_n,_\xi + q_m^{(I)}q_n^{(I)}\bar{\phi}_m,_\xi\,\bar{\phi}_n,_\xi\big]\Big\} \end{aligned} \tag{15}$$

$$\begin{aligned} \varepsilon_y^{(I)} &= v,_y^{(I)} + \tfrac{1}{2}\left[w,_y^{(I)}\right]^2 \\ &= -\left(\frac{h}{b}\right)^2 \Big\{-S + V_m\varphi,_\eta + V_m^{(I)}\bar{\varphi},_\eta + q_m g_m,_\eta \\ &\quad + \tfrac{1}{2}\big[q_m q_n\phi_m,_\eta\,\phi_n,_\eta + q_m q_n^{(I)}\phi_m,_\eta\,\bar{\phi}_n,_\eta \\ &\quad + q_m^{(I)}q_n\bar{\phi}_m,_\eta\,\phi_n,_\eta + q_m^{(I)}q_n^{(I)}\bar{\phi}_m,_\eta\,\bar{\phi}_n,_\eta\big]\Big\} \end{aligned} \tag{16}$$

$$\begin{aligned} \gamma_{xy}^{(I)} &= u,_y^{(I)} + v,_x^{(I)} + w,_x^{(I)}\,w,_y^{(I)} \\ &= -\left(\frac{h^2}{ab}\right)\big[U_m\psi,_\eta + U_m^{(I)}\bar{\psi},_\eta + V_m\varphi,_\xi + V_m^{(I)}\bar{\varphi},_\xi + q_m f_m,_\eta \\ &\quad + q_m q_n\phi_m,_\xi\,\phi_n,_\eta + q_m q_n^{(I)}\phi_m,_\xi\,\bar{\phi}_n,_\eta \\ &\quad + q_m^{(I)}q_n\bar{\phi}_m,_\xi\,\phi_n,_\eta + q_m^{(I)}q_n^{(I)}\bar{\phi}_m,_\xi\,\bar{\phi}_n,_\eta\big] \end{aligned} \tag{17}$$

where q_m, U_m, and V_m are generalized coordinates to be obtained. The strain energy density W is

$$2W = \{\varepsilon\}^T[A]\{\varepsilon\} + \{\kappa\}^T[D]\{\kappa\} \tag{18}$$

where

$$A_{kl} = hQ_{kl}, \qquad D_{kl} = \frac{h^3}{12}Q_{kl}$$

and where Q_{kl} are the components of the in-plane stiffness matrix of the plate. The total strain energy is obtained by integrating the strain energy density function:

$$U = \frac{1}{2}\int_0^a \int_0^b (\{\varepsilon\}^T[A]\{\varepsilon\} + \{\kappa\}^T[D]\{\kappa\})\,dx\,dy \qquad (19)$$

Since the forced displacement is applied on the loading edge, no external work exists, and the theory of minimum potential energy is equivalent to the minimum strain energy.

By substituting Eqs. (12–17) into Eq. (19) and neglecting the higher order terms, strain energy increase ΔU due to the transverse deflection is symbolically written as a quadratic function of generalized coordinates. The complete expression of the right-hand side of Eq. (19) is written in Appendices A and B. After some algebraic manipulation, ΔU can be symbolically written as

$$\Delta U = \boldsymbol{A}_{ij}s_i s_j + \boldsymbol{B}_{ij}t_i t_j + \boldsymbol{C}_{ij}t_i s_j + S\boldsymbol{D}_{ij}s_i s_j \qquad (20)$$

where the parameters s_i and t_i represent the terms relating to out-of-plane and in-plane directions, respectively, and the coefficients $\boldsymbol{A}_{ij}$, $\boldsymbol{B}_{ij}$, $\boldsymbol{C}_{ij}$, and $\boldsymbol{D}_{ij}$ can be derived from the equations in Appendices A and B.

By diffentiating Eq. (20) with respect to t_i and solving the equation derived with respect to t_i, we can express t_i in terms of s_i:

$$t_i = -\tfrac{1}{2}\boldsymbol{B}_{ik}^{-1}\boldsymbol{C}_{kj}s_j \qquad (21)$$

By substituting Eq. (21) into Eq. (20), we have the potential energy expressed only in terms of s_i,

$$\Delta U = \tilde{\boldsymbol{A}}_{ij}s_i s_j + S\boldsymbol{D}_{ij}s_i s_j \qquad (22)$$

where

$$\tilde{\boldsymbol{A}}_{ij} = \boldsymbol{A}_{ij} - \tfrac{1}{4}\boldsymbol{B}_{kl}^{-1}\boldsymbol{C}_{ki}\boldsymbol{C}_{lj}$$

By differentiating Eq. (22) by s_i, the buckling equation is obtained.

B. Constrained Point

As the two delaminated portions can move independently, the two delaminated surfaces may overlap each other as shown in Fig. 3a. To prevent the delaminated portions from overlapping, a constrained point is introduced as shown in Fig. 3b, where translational and rotational springs are assumed. The reaction force and moments at the constrained point (x_p, y_p) are given as

$$\begin{aligned} \bar{P}_z &= -\bar{K}_0[w^{(1)} - w^{(2)}] \\ \bar{M}_x &= -\bar{K}_x\left[w,_x^{(1)} - w,_x^{(2)}\right] \\ \bar{M}_y &= -\bar{K}_y\left[w,_y^{(1)} - w,_y^{(2)}\right] \end{aligned} \qquad (23)$$

where $\bar{K}_0$, $\bar{K}_x$, and $\bar{K}_y$ are the spring constants of the imaginary springs assumed at the constrained point and may be determined from the elastic properties of the plate, if necessary. When N constrained points $[(x_p, y_p)\ (p = 1, 2, \ldots, N)]$ are assumed, the strain energy change is

$$\begin{aligned} \Delta\tilde{U} = \Delta U + \frac{1}{2}\sum_{p=1}^{N}\Big\{&\bar{K}_0[w_1(x_p, y_p) - w_2(x_p, y_p)]^2 \\ &+ \bar{K}_x[w_{1,x}(x_p, y_p) - w_{2,x}(x_p, y_p)]^2 \\ &+ \bar{K}_y[w_{1,y}(x_p, y_p) - w_{2,y}(x_p, y_p)]^2\Big\} \end{aligned} \qquad (24)$$

After the normalization, the reaction force and moments are developed with the generalized coordinates $q_m^{(l)}$

$$\begin{aligned} P_z &= -K_0\left[q_m^{(1)} - q_m^{(2)}\right]\phi_m(\xi_p, \eta_p) \\ M_x &= -K_x\left[q_m^{(1)} - q_m^{(2)}\right]\phi_{m,\xi}(\xi_p, \eta_p) \\ M_y &= -K_y\left[q_m^{(1)} - q_m^{(2)}\right]\phi_{m,\eta}(\xi_p, \eta_p) \end{aligned} \qquad (25)$$

The values of nondimensional spring constants of $K_0 = \bar{K}_0 ab/D_{11}$, $K_x = \lambda^{-1}\bar{K}_x/D_{11}$, and $K_y = \lambda\bar{K}_y/D_{11}$ are given according to the convergence of the solution. The effect of the value K_0 becomes negligible when those values are large enough. The values of K_x and K_y do not affect the final solution if the position of the constrained point, where no rotational moments exist, is obtained.

The buckling analysis is performed without constraint, and the solution is examined whether it is physically admissible or not. If the solution is not admissible, a constrained point is applied at a center of an overlapped area. The eigenvalue problem is solved again. The contact point is moved by $\Delta\xi$ and $\Delta\eta$ according to the values of the following equation derived from the current solution so that the moments M_x and M_y become smaller,

$$\begin{aligned} \Delta\xi &= s_x M_x/P_z \\ \Delta\eta &= s_y M_y/P_z \end{aligned} \qquad (26)$$

where s_x and s_y are arbitrary constants that are determined according to the state of the convergence. In the present analysis, 0.5 is given for s_x and s_y. It should be noted that the buckling mode considered may not correspond to the smallest eigenvalue any more, because there can exist lower eigenvalues whose eigenmodes satisfy the constraints at the constrained points but are not physically admissible. The procedure is repeated until the movements $\Delta\xi$ and $\Delta\eta$ become small enough. In the present analysis, 10^{-4} is used. The contact point with very small relative displacement and slopes can be found after 10 to 20 steps. When the relative slopes become very small, the location of the contact point is decided to be obtained.

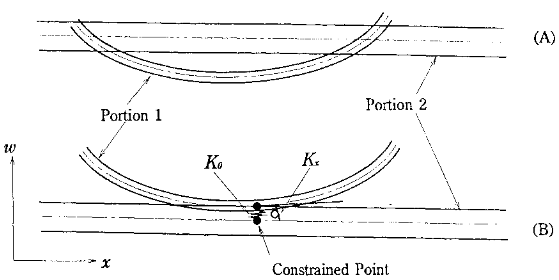

Fig. 3 Overlapped area and constrained point.

III. Experiment

Plain woven carbon fiber-reinforced composite plates (Toray T300/epoxy, 16 plies, $V_f \approx 50\%$) with one delamination are prepared for the experiment. The elastic properties E_L, E_T, ν_{LT}, and G_{LT} are measured and listed in Table 1. The suffices L and T denote the loading and the transverse directions, respectively. As the plane woven fabric plates are used, the bending-stretching coupling can be neglected even at the delaminated portions. The delamination is introduced by placing a thin polymer film (0.06-mm thick) between the corresponding interlaminar portion. Test specimens shown in Fig. 4 are cut out from the 300 × 300 mm plate. Two steel caps are glued on the loading edges of the specimen to realize the simply supported boundary condition. The delamination width α and location γ and the plate thickness h are listed in Table 2.

The specimen is set in a test machine (Shimadzu, autograph 10-TB) as shown in Fig. 5 and pushed very slowly with a crosshead

Table 1 Material properties

E_L, GPa	61.7
E_T, GPa	61.7
ν_{LT}	0.046
G_{LT}, GPa	5.17

Table 2 Parameters of specimens

Location γ	Width α	Thickness, mm
—	0	3.49
0.125	0.125	3.48
	0.25	3.47
	0.5	3.48
0.25	0.125	3.48
	0.25	3.47
	0.5	3.48
0.5	0.125	3.46
	0.25	3.47
	0.5	3.44

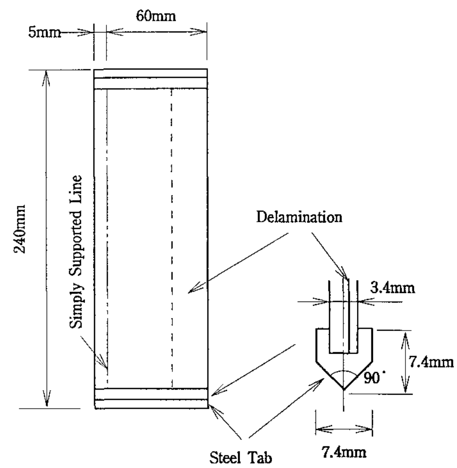

Fig. 4 Specimen.

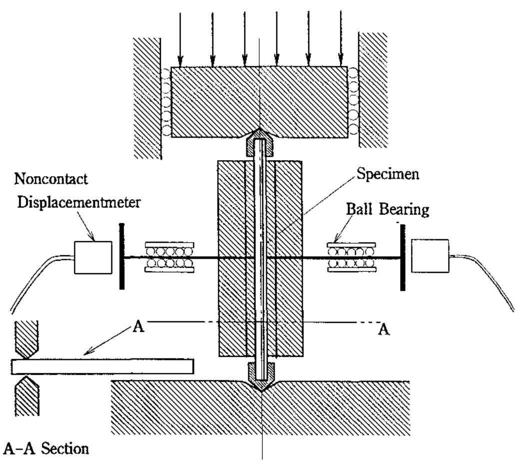

Fig. 5 Experimental apparatus.

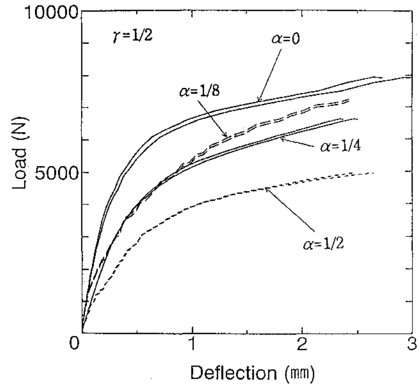

Fig. 6 Load and deflection at the center of the free edge ($\gamma = \frac{1}{2}$).

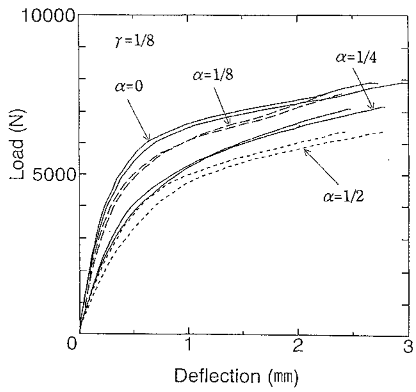

Fig. 7 Load and deflection at the center of the free edge ($\gamma = \frac{1}{8}$).

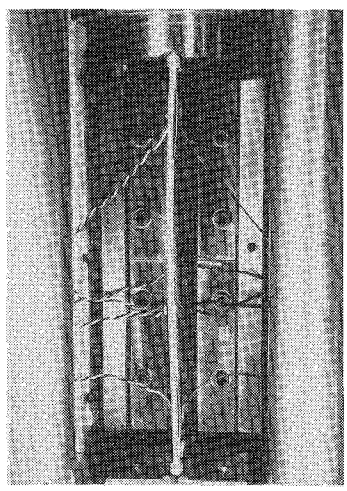

Fig. 8 The deformed shape of a locally buckled plate ($\gamma = \frac{1}{8}$ and $\alpha = \frac{1}{2}$).

speed of 0.1 mm/min. The deflections of both delaminated portions of the specimen are measured at the center of the free edge by using noncontact displacement meter (Emic, NPA-100) with a special attention in order not to disturb the deformation, because the delaminated strip is thin and sensitive to lateral force. Two steel dishes supported by ball bearings have very little resistance in the horizontal movement. The test data are stored in a personal computer and analyzed after the experiment. The specimen without a delamination buckles at about 7.1×10^3 N in a symmetric shape, which is about 4% higher than the theoretical one. The difference is thought to be caused mainly by incomplete simply supported condition of the side edge, which is supported by two steel edges as shown in Fig. 5. Friction between the plate surface and the edges causes some resistance to the rotation of the side edge and makes the buckling loads higher than ideal ones. The load-deflection curves obtained from the experiments are plotted in Figs. 6 and 7 for the cases of $\gamma = \frac{1}{2}$ and $\gamma = \frac{1}{8}$. Very little opening of the delamination is observed when $\gamma = \frac{1}{2}$. A shallower load increase is observed in the postbuckling region. The apparent stiffness is same for all of the cases. Since it was very difficult to adjust the alignment of the edges of the simply supported loading sides, the effect of the initial imperfection was not very small, and some increase of the deflection is observed even in the low-load region before the buckling. Some opening is found in the upper and lower portions of the specimen when $\gamma = \frac{1}{8}$ and $\alpha = \frac{1}{2}$. The buckled mode is shown in Fig. 8. The load-strain curve of Fig. 9 also shows the local buckling behavior. The buckling load is determined from the curve of the load to squared deflection of the representative point, that is, by the use of so-called δ^2 method.[17]

IV. Results and Discussion

When the bending-stretching coupling does not exist, the buckling analysis can be performed. Since only the symmetric deformation is observed in the experiment, symmetric mode function series about η

Table 3 Convergence of the buckling loads ($\alpha = 0.5$ and $\gamma = 0.5$); m and n are the numbers of the mode functions in x and y directions

m	n	S_{cr}/S_{cr0}
1	3	0.62187
2	3	0.62093
3	3	0.62070
4	3	0.62050
3	1	0.63190
3	2	0.62341
3	3	0.62070
3	4	0.61928
3	5	0.61846

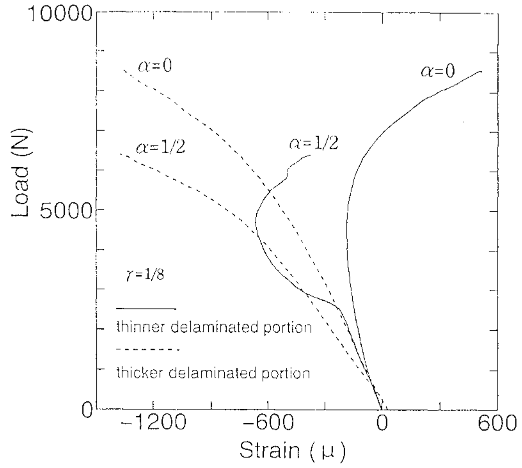

Fig. 9 Load and strains at the center of both sides near the free edge ($\gamma = \frac{1}{8}$).

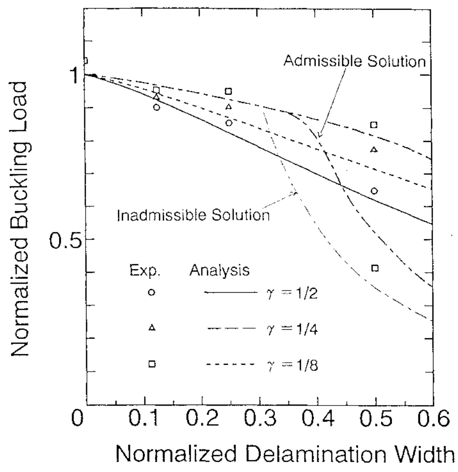

Fig. 10 Normalized buckling load and delamination width α.

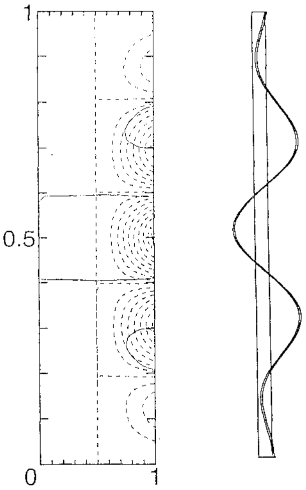

Fig. 11 Inadmissible buckling mode.

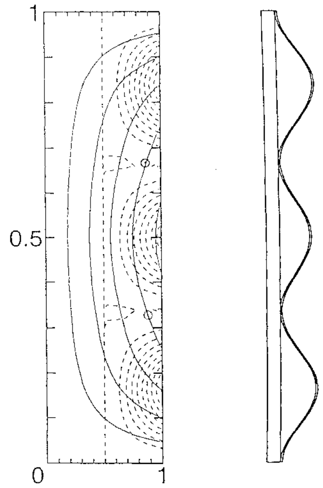

Fig. 12 Admissible buckling load obtained by the use of a constrained point.

coordinate are used for w and u and antisymmetric ones for v in the analysis. The convergence of the analytical results is examined for the plate with a delamination of $\alpha = 0.5$ and $\gamma = 0.5$ by increasing the number of the mode functions in x and y directions. The results are listed in Table 3. The numbers of mode functions for the in-plane displacements in each undelaminated and delaminated portions are set $4 \times 5 = 20$, that is, 60 degrees of freedom are used to develop u and v, respectively. In Table 3, the buckling load is normalized by S_{cr0}, which is the buckling load of the plate without a delamination. The convergence is very smooth. The lowest three modes in the x direction are sufficient to obtain the buckling loads. In the y direction, the result obtained also by using four lowest symmetric modes seems accurate enough. So the buckling analysis is performed by using lowest 3×4 mode functions in each undelaminated and delaminated portions, that is, 36 degrees of freedom are used for the out-of-plane deflection. When the local buckling is analyzed and a contact problem occurs, 4×5 functions are used for each portion, because a more complex deformed shape is expected to appear.

Figure 10 shows the relations between the buckling load and the delamination size α. The buckling load is normalized by the theoretical buckling load of the plate without a delamination. The experimental data agree very well with the present analysis. The results of a center delamination ($\gamma = \frac{1}{2}$) show the largest reduction of the buckling load, which reaches about 40% of the undelaminated plate when $\alpha = 0.5$. The global buckling loads decrease linearly with the size of delamination α in all cases. The reduction of the buckling load becomes smaller when the delamination is located closer to the plate surface. The local instability is observed when $\gamma = \frac{1}{8}$ and $\alpha > 0.33$. The solution plotted by a thin chain line is obtained without constraint. It has a shorter wave length in the y direction and is physically inadmissible. Figure 11 shows the buckling mode, which has a shape with five half-waves and overlapping in the delaminated portion. The thick chain line is a physically admissible solution, which is obtained by the use of the constrained points. Figure 12 is a typical deformed shape of the plate of $\alpha = 0.5$ and $\gamma = \frac{1}{8}$. The small circle is the position of the constrained point ($K_0 = 100$, $K_x = K_y = 20$). The buckling loads are, of course, a little higher than those without constraint. The buckling mode obtained does not coincide with the experimental one, which closes at its center. It is caused by the difference of the boundary condition along the delamination front. The process of the convergence is explained in Figs. 13–15. The stiffer the constrained spring is made, the higher the buckling stress becomes. However, the increase becomes negligible when $K_0 > 10$. The position of the constrained point influences little on the buckling load. The convergence of the buckling load can be said to occur more rapidly than that of the position.

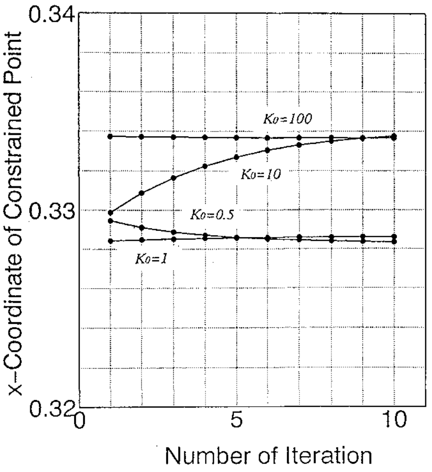

Fig. 13 Convergence phenomena of position $\bar{\xi}_p$ of the constrained point with the magnitude of the spring of constrained point.

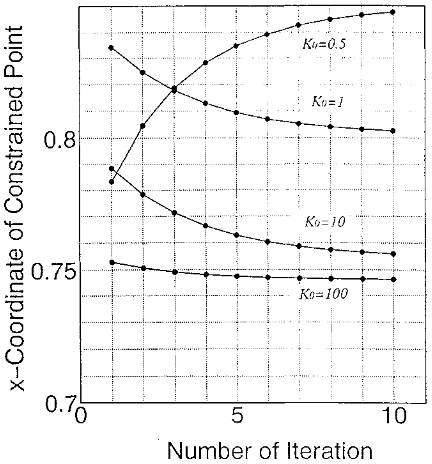

Fig. 14 Convergence phenomena of position η_p with the magnitude of the spring and location of the constrained point.

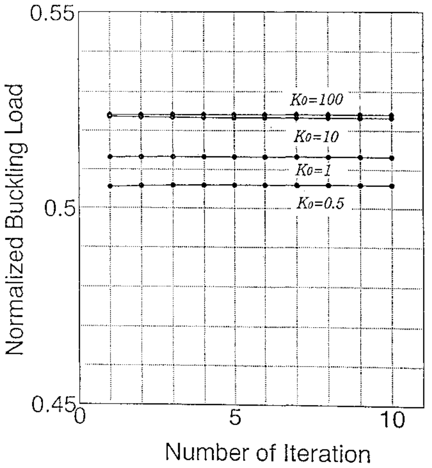

Fig. 15 Convergence phenomena of buckling load with the magnitude of the spring and location of the constrained point.

The local instability load, which is very low, does not coincide with global instability of the plate. However, the opening may be very important, because it may cause a propagation of the delamination.

V. Conclusion

A classical Rayleigh–Ritz analysis and an experimental work are performed to study the effect of an edge delamination on compressive behaviors of composite plates with one free edge, which is a simplified model of a stiffener panel of a stiffened plate. Through the present studies, we have the following conclusions:

1) An efficient analytical scheme to estimate buckling loads of plates with an edge delamination is developed.

2) The global buckling load reduction due to an edge delamination is significant. The buckling load decreases proportional to the width of the delamination.

3) The global instability load of the plate with same size delamination becomes smallest when the delamination locates on the midplane.

4) The local instability is observed at the delaminated portion when the delamination is located near the surface and its size is relatively large. A contact problem must be considered in this case.

Appendix A: Strain Energy Relating to Bending Components

$$
\begin{aligned}
&\frac{1}{2}\int_0^a\int_0^b \{\kappa\}^T[D]\{\kappa\}\,\mathrm{d}x\,\mathrm{d}y \\
&= \frac{h^2}{2ab}\Bigg(\Bigg[q_m q_n\Bigg\{\lambda^2 D_{11}\int_0^1\int_0^{\bar{\alpha}} \phi_{m,\xi\xi}\,\phi_{n,\xi\xi}\,\mathrm{d}\xi\,\mathrm{d}\eta \\
&+2D_{12}\int_0^1\int_0^{\bar{\alpha}} \phi_{m,\xi\xi}\phi_{n,\eta\eta}\,\mathrm{d}\xi\,\mathrm{d}\eta \\
&+\lambda^{-2}D_{22}\int_0^1\int_0^{\bar{\alpha}} \phi_{m,\eta\eta}\,\phi_{n,\eta\eta}\,\mathrm{d}\xi\mathrm{d}\eta \\
&+4D_{66}\int_0^1\int_0^{\bar{\alpha}} \phi_{m,\xi\eta}\,\phi_{n,\xi\eta}\,\mathrm{d}\xi\mathrm{d}\eta \\
&+\sum_{I=1}^{2}\Bigg[\lambda^2 D_{11}^{(I)}\int_0^1\int_{\bar{\alpha}}^1 \phi_{m,\xi\xi}\,\phi_{n,\xi\xi}\,\mathrm{d}\xi\mathrm{d}\eta \\
&+2D_{12}^{(I)}\int_0^1\int_{\bar{\alpha}}^1 \phi_{m,\xi\xi}\,\phi_{n,\eta\eta}\,\mathrm{d}\xi\mathrm{d}\eta \\
&+\lambda^{-2}D_{22}^{(I)}\int_0^1\int_{\bar{\alpha}}^1 \phi_{m,\eta\eta}\,\phi_{n,\eta\eta}\,\mathrm{d}\xi\mathrm{d}\eta \\
&+4D_{66}^{(I)}\int_0^1\int_{\bar{\alpha}}^1 \phi_{m,\xi\eta}\,\phi_{n,\xi\eta}\,\mathrm{d}\xi\mathrm{d}\eta\Bigg]\Bigg\} \\
&+2\sum_{I=1}^{2} q_m q_n^{(I)}\Bigg[\lambda^2 D_{11}^{(I)}\int_0^1\int_{\bar{\alpha}}^1 \phi_{m,\xi\xi}\,\bar{\phi}_{n,\xi\xi}\,\mathrm{d}\xi\mathrm{d}\eta \\
&+D_{12}^{(I)}\int_0^1\int_{\bar{\alpha}}^1 (\phi_{m,\xi\xi}\,\bar{\phi}_{n,\eta\eta}+\phi_{m,\eta\eta}\,\bar{\phi}_{n,\xi\xi})\mathrm{d}\xi\mathrm{d}\eta \\
&+\lambda^{-2}D_{22}^{(I)}\int_0^1\int_{\bar{\alpha}}^1 \phi_{m,\eta\eta}\,\bar{\phi}_{n,\eta\eta}\,\mathrm{d}\xi\mathrm{d}\eta \\
&+4D_{66}^{(I)}\int_0^1\int_{\bar{\alpha}}^1 \phi_{m,\xi\eta}\,\bar{\phi}_{n,\xi\eta}\,\mathrm{d}\xi\mathrm{d}\eta\Bigg] \\
&+\sum_{I=1}^{2} q_m^{(I)} q_n^{(I)}\Bigg[\lambda^2 D_{11}^{(I)}\int_0^1\int_{\bar{\alpha}}^1 \bar{\phi}_{m,\xi\xi}\,\bar{\phi}_{n,\xi\xi}\,\mathrm{d}\xi\mathrm{d}\eta \\
&+2D_{12}^{(I)}\int_0^1\int_{\bar{\alpha}}^1 \bar{\phi}_{m,\xi\xi}\,\bar{\phi}_{n,\eta\eta}\,\mathrm{d}\xi\mathrm{d}\eta \\
&+\lambda^{-2}D_{22}^{(I)}\int_0^1\int_{\bar{\alpha}}^1 \bar{\phi}_{m,\eta\eta}\,\bar{\phi}_{n,\eta\eta}\,\mathrm{d}\xi\mathrm{d}\eta \\
&+4D_{66}^{(I)}\int_0^1\int_{\bar{\alpha}}^1 \bar{\phi}_{m,\xi\eta}\,\bar{\phi}_{n,\xi\eta}\,\mathrm{d}\xi\mathrm{d}\eta\Bigg]\Bigg)
\end{aligned}
$$

Appendix B: Strain Energy Relating to In-Plane Components

$$\frac{1}{2}\int_0^a\int_0^b \{\varepsilon\}^T[A]\{\varepsilon\}\mathrm{d}x\mathrm{d}y$$

$$= \frac{h^4}{2ab}\left(\lambda^{-2}\left(A_{22} - \frac{A_{12}{}^2}{A_{11}}\right)S^2\right.$$

$$+\lambda^{-2}S\left\{\left(A_{22} - \frac{A_{12}{}^2}{A_{11}}\right)q_m q_n \int_0^1\int_0^1 \phi_{m,\eta}\,\phi_{n,\eta}\,\mathrm{d}\xi\,\mathrm{d}\eta\right.$$

$$+\sum_{I=1}^{2}\left[A_{22}^{(I)} - \frac{A_{12}^{(I)2}}{A_{11}^{(I)}}\right]\left[2q_m q_n^{(I)}\int_0^1\int_{\bar{\alpha}}^1 \phi_{m,\eta}\,\bar{\phi}_{n,\eta}\,\mathrm{d}\xi\,\mathrm{d}\eta\right.$$

$$\left.\left.+q_m^{(I)}q_n^{(I)}\int_0^1\int_{\bar{\alpha}}^1 \bar{\phi}_{m,\eta}\,\bar{\phi}_{n,\eta}\,\mathrm{d}\xi\,\mathrm{d}\eta\right]\right\}$$

$$+q_m q_n\left\{\sum_{I=1}^{2}k_I{}^2\left[\lambda^{-2}A_{22}^{(I)}\int_0^1\int_{\bar{\alpha}}^1 g_{m,\eta}\,g_{n,\eta}\,\mathrm{d}\xi\,\mathrm{d}\eta\right.\right.$$

$$\left.\left.+A_{66}^{(I)}\int_0^1\int_{\bar{\alpha}}^1 f_{m,\eta}\,f_{n,\eta}\,\mathrm{d}\xi\,\mathrm{d}\eta\right]\right\}$$

$$+\sum_{I=1}^{2}q_m U_n^{(I)}\left[k_I A_{12}^{(I)}\int_0^1\int_{\bar{\alpha}}^1 g_{m,\eta}\,\bar{\varphi}_{n,\xi}\,\mathrm{d}\xi\,\mathrm{d}\eta\right]$$

$$+\sum_{I=1}^{2}q_m V_n^{(I)}k_I\left[\lambda^{-2}A_{22}^{(I)}\int_0^1\int_{\bar{\alpha}}^1 g_{m,\eta}\,\bar{\theta}_{n,\eta}\,\mathrm{d}\xi\,\mathrm{d}\eta\right.$$

$$\left.+A_{66}^{(I)}\int_0^1\int_{\bar{\alpha}}^1 f_{m,\eta}\,\bar{\theta}_{n,\xi}\,\mathrm{d}\xi\mathrm{d}\eta\right]$$

$$+U_m U_n\left(\lambda^2 A_{11}\int_0^1\int_0^1 \varphi_{m,\xi}\,\varphi_{n,\xi}\,\mathrm{d}\xi\,\mathrm{d}\eta\right.$$

$$\left.+A_{66}\int_0^1\int_0^1 \varphi_{m,\eta}\,\varphi_{n,\eta}\,\mathrm{d}\xi\,\mathrm{d}\eta\right)$$

$$+\sum_{I=1}^{2}U_m U_n^{(I)}\left[\lambda^2 A_{11}^{(I)}\int_0^1\int_0^1 \varphi_{m,\xi}\,\bar{\varphi}_{n,\xi}\,\mathrm{d}\xi\,\mathrm{d}\eta\right.$$

$$\left.+A_{66}^{(I)}\int_0^1\int_0^1 \varphi_{m,\eta}\,\bar{\varphi}_{n,\eta}\,\mathrm{d}\xi\,\mathrm{d}\eta\right]$$

$$+\sum_{I=1}^{2}U_m^{(I)}U_n^{(I)}\left[\lambda^2 A_{11}^{(I)}\int_0^1\int_0^1 \bar{\varphi}_{m,\xi}\,\bar{\varphi}_{n,\xi}\,\mathrm{d}\xi\,\mathrm{d}\eta\right.$$

$$\left.+A_{66}^{(I)}\int_0^1\int_0^1 \bar{\varphi}_{m,\eta}\,\bar{\varphi}_{n,\eta}\,\mathrm{d}\xi\,\mathrm{d}\eta\right]$$

$$+2U_m V_n\left(A_{12}\int_0^1\int_0^1 \varphi_{m,\xi}\,\theta_{n,\eta}\,\mathrm{d}\xi\,\mathrm{d}\eta\right.$$

$$\left.+A_{66}\int_0^1\int_0^1 \varphi_{m,\eta}\,\theta_{n,\xi}\,\mathrm{d}\xi\,\mathrm{d}\eta\right)$$

$$+2\sum_{I=1}^{2}U_m V_n^{(I)}\left[A_{12}^{(I)}\int_0^1\int_0^1 \varphi_{m,\xi}\,\bar{\theta}_{n,\eta}\,\mathrm{d}\xi\,\mathrm{d}\eta\right.$$

$$\left.+A_{66}^{(I)}\int_0^1\int_0^1 \varphi_{m,\eta}\,\bar{\theta}_{n,\xi}\,\mathrm{d}\xi\,\mathrm{d}\eta\right]$$

$$+2\sum_{I=1}^{2}U_m^{(I)}V_n\left[A_{12}^{(I)}\int_0^1\int_0^1 \bar{\varphi}_{m,\xi}\,\theta_{n,\eta}\,\mathrm{d}\xi\,\mathrm{d}\eta\right.$$

$$\left.+A_{66}^{(I)}\int_0^1\int_0^1 \bar{\varphi}_{m,\eta}\,\theta_{n,\xi}\,\mathrm{d}\xi\,\mathrm{d}\eta\right]$$

$$+2\sum_{I=1}^{2}U_m^{(I)}V_n^{(I)}\left[A_{12}^{(I)}\int_0^1\int_0^1 \bar{\varphi}_{m,\xi}\,\bar{\theta}_{n,\eta}\,\mathrm{d}\xi\,\mathrm{d}\eta\right.$$

$$\left.+A_{66}^{(I)}\int_0^1\int_0^1 \bar{\varphi}_{m,\eta}\,\bar{\theta}_{n,\xi}\,\mathrm{d}\xi\,\mathrm{d}\eta\right]$$

$$+V_m V_n\left(\lambda^{-2}A_{22}\int_0^1\int_0^1 \theta_{m,\eta}\,\theta_{n,\eta}\,\mathrm{d}\xi\,\mathrm{d}\eta\right.$$

$$\left.+A_{66}\int_0^1\int_0^1 \theta_{m,\xi}\,\theta_{n,\xi}\,\mathrm{d}\xi\,\mathrm{d}\eta\right)$$

$$+2\sum_{I=1}^{2}V_m V_n^{(I)}\left[\lambda^{-2}A_{22}^{(I)}\int_0^1\int_0^1 \theta_{m,\eta}\,\bar{\theta}_{n,\eta}\,\mathrm{d}\xi\,\mathrm{d}\eta\right.$$

$$\left.+A_{66}^{(I)}\int_0^1\int_0^1 \theta_{m,\xi}\,\bar{\theta}_{n,\xi}\,\mathrm{d}\xi\,\mathrm{d}\eta\right]$$

$$+\sum_{I=1}^{2}V_m^{(I)}V_n^{(I)}\left[\lambda^{-2}A_{22}^{(I)}\int_0^1\int_0^1 \bar{\theta}_{m,\eta}\,\bar{\theta}_{n,\eta}\,\mathrm{d}\xi\,\mathrm{d}\eta\right.$$

$$\left.+A_{66}^{(I)}\int_0^1\int_0^1 \bar{\theta}_{m,\xi}\,\bar{\theta}_{n,\xi}\,\mathrm{d}\xi\,\mathrm{d}\eta\right]$$

$$\left.+\text{(higher order terms)}\right)$$

Acknowledgments

The authors would like to express their sincere thanks to M. Ema and T. Toda for their effort to complete the experiment for their graduation thesis.

References

[1] Chai, H., and Babcock, C. D., "One Dimensional Modelling of Failure in Laminated Plates by Delamination Buckling," *International Journal of Solids and Structures*, Vol. 17, No. 11, 1981, pp. 1069–1083.

[2] Simitses, G. J., Sallam, S., and Yin, W. L., "Effects of Delamination of Axially Loaded Homogeneous Laminated Plates," *AIAA Journal*, Vol. 23, No. 9, 1985, pp. 1437–1444.

[3] Yin, W. L., Sallam, S. N., and Simitses, G. J., "Ultimate Axial Load Capacity of Delaminated Beam-Plate," *AIAA Journal*, Vol. 24, No. 1, 1988, pp. 123–128.

[4] Yin, W. L., "The Effects of Laminated Structure on Delamination Buckling and Growth," *Journal of Composite Materials*, Vol. 22, June 1988, pp. 502–517.

[5] Vizzini, A. J., and Lagace, P. A., "The Buckling of a Delaminated Sublaminate on an Elastic Foundation," *Journal of Composite Materials*, Vol. 21, Dec. 1987, pp. 1106–1117.

[6] Kardomateas, G. A., "End Fixity Effects on the Buckling and Postbuckling of Delaminated Composites," *Composite Science and Technology*, Vol. 34, No. 2, 1989, pp. 113–128.

[7] Wang, S. S., Zahlan, N. M., and Suemasu, H., "Compressive Stability of Delaminated Random Short-Fiber Composite, Part I—Modeling and Methods of Analysis," *Journal of Composite Materials*, Vol. 19, July 1985, pp. 296–316.

[8] Wang, S. S., Zahlan, N. M., and Suemasu, H., "Compressive Stability of Delaminated Random Short-Fiber Composite, Part II—Experimental and Analytical Results," *Journal of Composite Materials*, Vol. 19, July 1985, pp. 317–333.

[9] Suemasu, H., "Effects of Multiple Delaminations on Compressive Buckling Behaviors of Composite Panels," *Journal of Composite Materials*, Vol. 27, No. 12,1993, pp. 1172–1192.

[10] Suemasu, H., "Postbuckling Behaviors of Composite Panels with Mul-

tiple Delaminations," *Journal of Composite Materials*, Vol. 27, No. 11, 1993, pp. 1077–1096.
[11]Chai, H., and Babcock, C. D. "Two-Dimensional Modelling of Compressive Failure in Delaminated Laminates," *Journal of Composite Materials*, Vol. 19, Jan. 1985, pp. 67–98.
[12]Whitcomb, J. D., and Shivakumar, K. N., "Strain-Energy Release Rate Analysis of Plates With Postbuckled Delaminations," *Journal of Composite Materials*, Vol. 23, July 1989, pp. 714–734.
[13]Suemasu, H., "Compressive Behaviors of Composite Panels with a Delamination," *Proceedings of Fifth Japan-U.S. Conference on Composite Materials*, Tama-City, Tokyo, 1990, pp. 637–644.
[14]Suemasu, H., "Analytical Study of Shear Buckling and Postbuckling Behaviors of Composite Plates with a Delamination," *JSME International Journal Series I*, Vol. 34, No. 2, 1991, pp. 135–142.
[15]Suemasu, H., "Compressive Behavior of Fiber Reinforced Composite Plates with a Center Delamination," *Advanced Composite Materials*, Vol. 1, No. 1, 1991, pp. 23–37.
[16]Shahwan, and Waas, "A Mechanical Model for the Buckling of Unilaterally Constrained Rectangular Plates," *International Journal of Solids and Structures*, Vol. 31, No. 1, 1994, pp. 23–37.
[17]Kobayashi, S., *Airplane Structure Mechanics*, Maruzen, Tokyo, 1992, pp. 141–156 (in Japanese).